FULL PAPER

Bio-derived carbon nanofibers from lignin as high performance Li-ion anode materials

Mario Culebras[a]*, Hugh Geaney[b], Anne Beaucamp[a], Prathviraj Upadhyaya[a], Eric Dalton[a], Kevin M. Ryan[b] and Maurice N. Collins[a]

Abstract: Development of cost effective and increasingly efficient sustainable materials for energy storage devices, such Li ion batteries, is of crucial future importance. Herein, the preparation of carbon nanofibers from biopolymer blends of lignin (by-product from the paper and pulp industry), with polylactic acid (PLA) and a thermoplastic elastomeric polyurethane (TPU) are described. Scanning electron microscopy (SEM) analysis shows the evolving microstructural morphology after each processing step, (electrospinning, stabilization and carbonization). Importantly, it is possible to tailor nanofiber porosity utilising miscibility/immiscibility rules between lignin and the polymer additive (PLA/TPU). PLA blends (immiscible) generate porous structures while miscible lignin/TPU blends are solid when carbonised. Electrodes produced from 50 % of PLA blends have capacity values of 611 $mAhg^{-1}$ after 500 charge/discharge cycles; the highest reported to date for sustainable electrodes for Li-ion batteries. Thus, this work will promote the development of lignocelluose waste materials as high performace energy storage materials.

.

Introduction

Energy storage devices are underpinning the rapid development of modern society. Multifunctional portable electronic devices such as smartphones, laptops, tablets and biomedical sensing equipment require efficient and cost-effective energy storage devices such as batteries and supercapacitors in order to meet their ever increasing energy demands. Coupled to this, the increasing demand for electric vehicles, has dictated the necessity to investigate new materials for energy storage devices [2-5]. Lithium-ion batteries (LIBs) are the most efficient energy storage devices and are widely used in electronic devices and electric vehicles [6-8]. Carbon materials such as carbon black and graphite are used in commercial LIB anodes due to their availability, processability and long-term cycling stability. However, one of the main problems associated with graphite is its low energy density, with its theoretical capacity of just 372 $mAhg^{-1}$. For this reason, many studies have been focused on finding new carbon based materials to be used as anodes in LIBs[3, 11]. Carbon nanostructures including graphene, carbon nanotubes and mesoporous carbon have been studied as alternatives to graphite, exhibiting enhanced Li storage capacities and enhanced performance [12-18]. However, their high cost and limited production throughput make their integration into industrial production difficult compared to traditional graphite. Carbon nanofibers produced by electrospinning can be incorporated into the commercial production of LIBs due to their lower cost (compared to CNTs or graphene) and the possibility of producing electrodes with large areas [1, 9-10, 19-20]. However, the vast majority of carbon fibres are produced using polyacrylonitrile (PAN) as precursor material. PAN is a petroleum based polymer with serious drawbacks such as: high production cost and environmental issues associated with high CO_2 emissions and solvent usage during synthesis [22]. Lignin is considered a viable sustainable alternative to PAN as carbon fibre precursor [23-28]. Lignin is the most abundant aromatic biopolymer on the planet. It is amorphous and is present in the cell wall of plants. Currently, it is a non-valorised waste from the paper and pulp industry, and its degradation generates furans and dioxins which consume dioxygen [30-31]. The aromatic molecular structure of lignin generated by the condensation of the three different monolignols (coniferyl alcohol, sinapyl alcohol and p-coumaryl alcohol) renders it ideal for carbon fibre production [25]. However, its low molecular weight causes serious processing issues whilst electrospinning, as its low viscosity requires the addition of petroleum based polymers such as PAN or high molecular weight polyethylene oxide[35-36].

In the present study, we have developed fully sustainable carbon nanofibres with differing tailored microstructures using lignin blended with two biobased polymers, a thermoplastic elastomer polyurethane (TPU) and polylactic acid (PLA). The method allows for the formation of porous structures depending on the miscibility of the polymer additive. Completely miscible blends (Lignin/TPU) provide homogenous structures while immiscible (Lignin/PLA) blends phase separation providing porous structures after carbonization. In order to promote lignin crosslinking and avoid its melting, methylene diphenyl diisocyanate (MDI) was used as a crosslinking agent during stabilization immediately prior to carbonisation. Thus, we propose a sustainable anode material for LIBs, utilising biobased materials that offer microstructure tunability, leading to better performance compared to current state of the art and commercial materials.

Results and Discussion

Pure lignin solutions display a very low viscosity due to the low molecular weight of lignin and are therefore unsuitable for electrospinning **[23]**. As a result, lignin blends were developed. For the case of lignin/PLA blends, a mixture of solvent, DMF:THF (1:1 w/w), is required since phase separation occurs when only one

[a] *Stokes Laboratories, Bernal Institute, University of Limerick, (Ireland)*
[b] *Bernal Institute & Chemical Sciences Department, University of Limerick* † Footnotes relating to the title and/or authors should appear here.
Electronic Supplementary Information (ESI) available: [additional thermogravimetric analysis, structural and electrochemical characterisation].

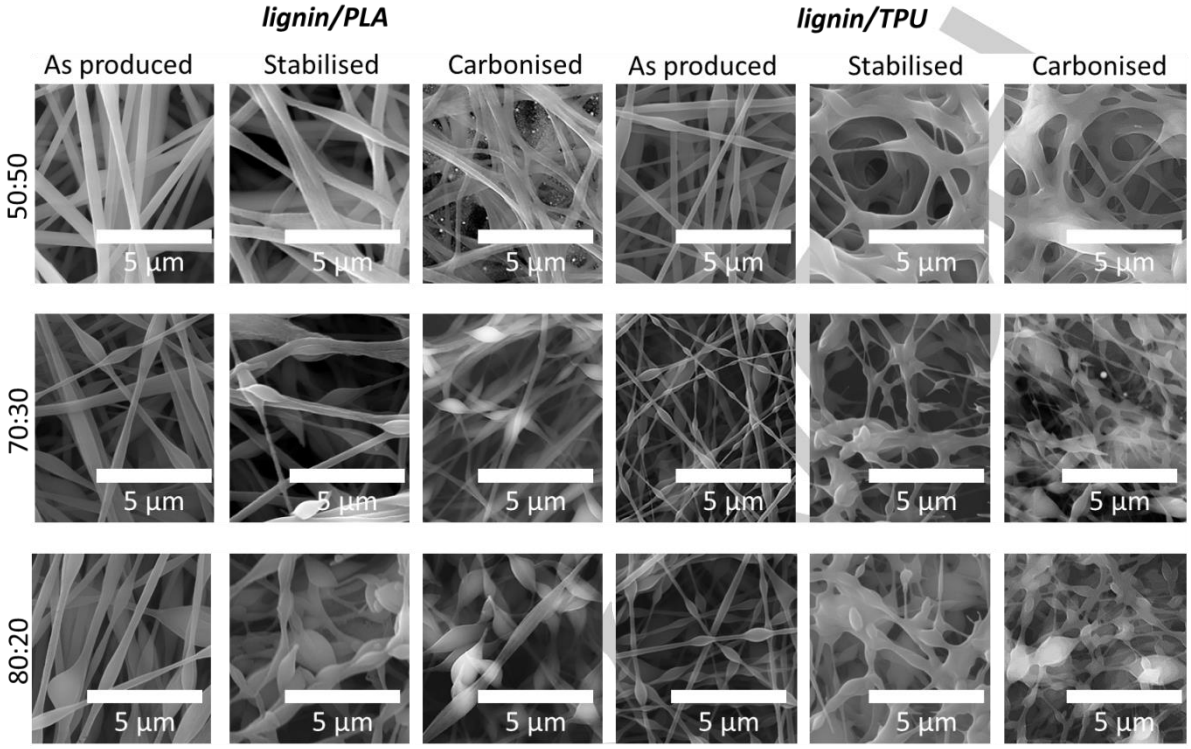

Figure 1. SEM images of Lignin based nanofibers after each processing step as a function of their composition

solvent is utilized. Figure 1 shows the evolution of the morphology after each step of the electrode production process i.e., electrospinning, stabilisation and carbonisation. The stabilisation process coverts thermoplastic lignin blends into thermoset crosslinked polymers, and this is key to avoid melting during carbonisation. Lignin/PLA nanofibres exhibit diameter between 400-600 nm, 200-400 nm and 200-500 nm for PLA contents of 50 %, 30 % and 20 % respectively. For lignin/PLA samples, the beading degree increased with lignin content, with 50 % PLA being the optimum composition to minimize beading along the nanofibres. Lignin/TPU nanofibres depicted the same trend, with beading degree increasing as the TPU content decreased. However, the TPU samples show a higher beading degree compared to the analogous PLA samples.

After the stabilization step, melting is observed (see Figure 1) particularly prevalent in TPU samples. However, lignin/PLA-50:50 and lignin/PLA-70:30 remain intact and this is largely attributed to more efficient crosslinking reactions. The stabilisation step is known to be technically challenging for easily meltable lignin. For this reason, previous studies have used very slow heating ramp rates of 0.1 ºC/min for stabilisation of lignin based microfibers [23]. In this work, several isothermal steps were combined to prevent melting of the nanofibers during the stabilisation step. However, the addition of MDI as crosslinker was crucial in order to maintain the shape of the nanofibers. (see Figure S1). Crosslinking occurs between lignin hydroxyl groups and MDI isocyanate groups, as shown in Figure 2, generating urethane groups linking lignin molecules together, thereby transitioning from thermoplastic to thermoset during the stabilization. The resulting urethane groups have been identified using FTIR (see supporting information Figure S2)

After carbonisation the morphology of the nanofibers remain unchanged keeping the shape obtained after the stabilisation step. lignin/PLA-50:50 displays the best shape and morphology retention producing well defined nanofibers around the whole surface of the electrode.Previous studies have shown that phase separation occurs between lignin and PLA. Consequently, two different structures are obtained after carbonisation as can be

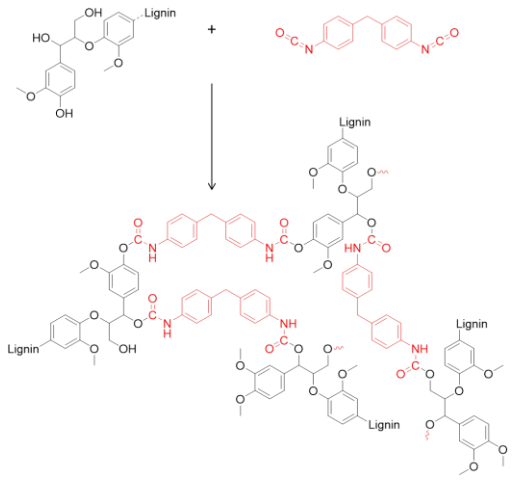

Figure 2. Simplified chemical structure of lignin after crosslinking reactions.

[a] *Stokes Laboratories, Bernal Institute, University of Limerick, (Ireland)*
[b] *Bernal Institute & Chemical Sciences Department, University of Limerick* † Footnotes relating to the title and/or authors should appear here.
Electronic Supplementary Information (ESI) available: [additional thermogravimetric analysis, structural and electrochemical characterisation].

observed in Figure 3. The phase separation between lignin and PLA generates a porous structure after carbonisation (Figure 3(c)). The fact that PLA depolymerises and volatilises completely above 370ºC, means that it becomes a sacrificial polymer during the carbonisation process, generating pores along the carbon nanofibers. In contrast, for compatible blends (lignin/TPU) the morphology of the carbon nanofibers after carbonization is homogenous. In addition, this fact affects to carbon yield of the samples (see Table 1). Lignin/TPU samples showed higher carbon yields than Lignin/PLA due to both polymers (TPU and Lignin) contribute to the carbon phase.

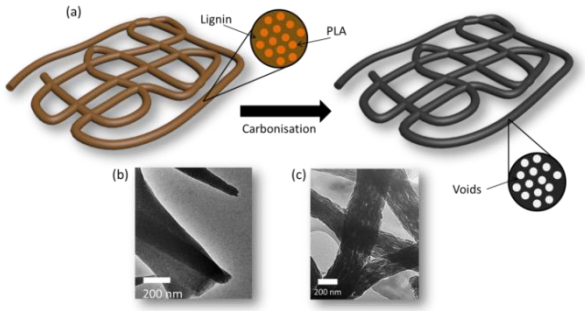

Figure 3. (a) Schematic of phase separation for TcA/PLA fibres. TEM images of (b) TcA/TPU-50:50 and (c) TcA/PLA-50:50.

Raman spectroscopy was carried out to provide crystallographic information on the carbon nanofibers as a function of precursor composition. The normalised Raman spectra for the CNFs are shown in Figure 4. The Raman spectra show two characteristic peaks centred at 1345 cm^{-1} and 1585 cm^{-1} the D-band and G-band

Table 1. Carbon yield of the nanofibres.

	Carbon Yield at 900ºC from stabilised samples (%)	
Composition (Weight %)	Lignin-TPU	Lignin-PLA
50-50	41	20.3
70-30	47.1	26.3
80-20	47.5	32.7

respectively [37]. The D-band indicates a disordered graphitic structure while the G-band is associated with sp2 vibrations of the ordered graphitic crystal [38] . All the spectra were analysed by deconvoluting the peaks using the Lorentzian function in order to provide the intensity of the D-band and G-bands. The ratios of the intensities of the D-band to the G-band, I_D/I_G (R) are shown in Table 2. Lower I_D/I_G values indicate higher graphitisation and alignment of the graphitic planes in carbonaceous materials [39]. Very similar values were obtained for the two blends although with different trends. For the porous carbon fibres the I_D/I_G ratio slightly increases with the percentage of PLA in the precursor material, indicating a less ordered graphitic structure. However, for TPU samples the trend was the opposite, indicating more ordered graphitic structure with increased TPU content. This fact can be explained due to the different miscibility of PLA and TPU with lignin. In Lignin/PLA blends, the phase separation process makes the graphitisation more difficult and alignment of the graphitic

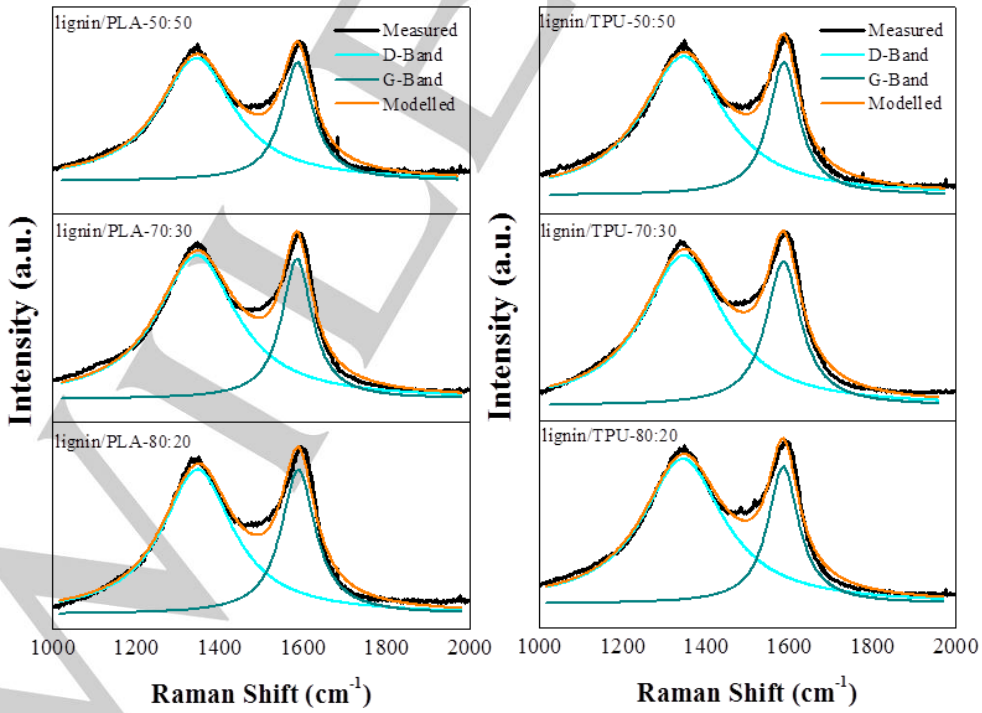

Figure 4. Deconvoluted Raman spectra of CNFs as a function of lignin composition.

[a] *Stokes Laboratories, Bernal Institute, University of Limerick, (Ireland)*
[b] *Bernal Institute & Chemical Sciences Department, University of Limerick* † Footnotes relating to the title and/or authors should appear here.
Electronic Supplementary Information (ESI) available: [additional thermogravimetric analysis, structural and electrochemical characterisation].

planes is compromised compared to completely miscible blends (lignin/TPU).

The graphitic crystallite domain size (L_a) can be estimated by the empirical formula proposed by Knight and White which describes the relationship between I_D/I_G and L_a as $L_a = 4.4/(I_D/I_G)$ [37]. Table 2 shows the La values of the carbon nanofibres for the different samples. The La values are slightly higher for the samples prepared with PLA based precursors, indicating larger graphite crystallites and in consequence higher graphitisation degree. This is due to only the lignin phase participation in the carbon formation. In contrast, lignin/TPU is a homogenous system, thus both components participate in carbon formation through possible condensation reactions between both polymers[23] that can produce a synergistic effect in the formation of the graphite crystals.

Table 2. D and G band position, relative intensities (R) and crystallite domain size La of CNFs produced from the different lignin blends

Sample	D band (cm^{-1})	G band (cm^{-1})	R (I_D/I_G)	La (nm)
Lignin/PLA-80:20	1346	1588	1	4.4
Lignin/PLA-70:30	1345	1585	1.03	4.29
Lignin/PLA-50:50	1344	1586	1.04	4.24
Lignin/TPU-80:20	1344	1585	1.06	4.16
Lignin/TPU-70:30	1345	1586	1.04	4.22
Lignin/TPU-50:50	1345	1587	1.04	4.22

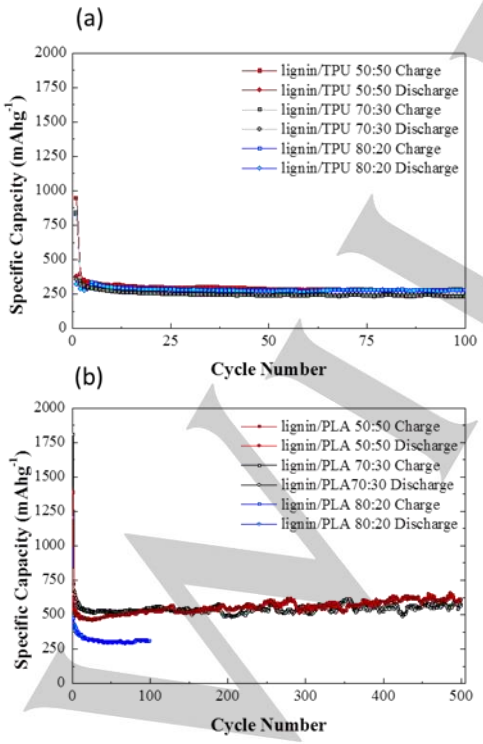

Figure 5. Gravimetric capacity values for extended cycling testing at C/2 rate for (a) TPU and (b) PLA based electrodes of different compositions.

Electrochemical testing of electrodes composed of electrospun lignin/TPU and lignin/PLA nanofibers was carried out galvanostatically at a rate of C/2. All of the lignin/TPU samples show stable cycling performance over 100 charge/discharge cycles (Figure 5 (a)), however the specific capacities of the anodes were below the theoretical capacity of graphite (372 $mAhg^{-1}$). For lignin/TPU 50:50 and lignin/TPU 80:20 the capacities were approximately 280 $mAhg^{-1}$ at this point, while lignin/TPU 70:30 was lower at 230 $mAhg^{-1}$. On the other hand, PLA nanofibers exhibited notably higher specific capacity values (Figure 5 (b)). In particular, it was found that PLA electrodes with 50:50 and 70:30 compositions exhibited extremely stable, long-term cycling performance. After 500 charge/discharge cycles, the specific capacities of the electrodes were 611 $mAhg^{-1}$ and 572 $mAhg^{-1}$ respectively, which is a strong improvement on the performance of conventional graphite and compares well with existing literature on conventional carbon nanofibers (Table 3). Analysis of the voltage profiles (Figure S3) and differential capacity plots (Figure S4 and S5) demonstrates that the first lithiation process in each case contained a peak related to the formation of a solid electrolyte interphase at approximately 1V. This peak was more pronounced for the samples formed using TPU. The enhanced specific capacity of the PLA composed nanofibers is primarily attributed to the increased porosity, according to BET experiments showed in Tables S3 (345 m^2g^{-1} for Lignin/TPU-50:50 compared to 670 m^2g^{-1} for Lignin/PLA-50:50 carbon nanofibers), leading to additional sites for Li storage as previously reported for PPy [21] and PAN[10] derived carbon nanofibers. However, the lack of shape retention in the 80:20 sample significantly decreases the electrochemical performance compared to the samples with a well-defined fibre structure (lignin/PLA 70:30 and 50:50), see Figure 1.

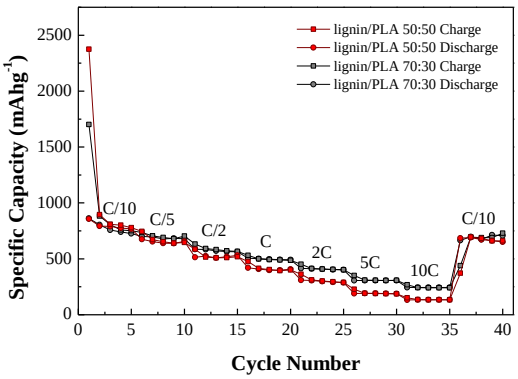

Figure 6. Rate capability test for PLA 70:30 and PLA 50:50 electrode at various rates.

To further investigate the best performing PLA derived nanofibers (i.e. 50:50 and 70:30), rate capability testing was carried out from C/10 to 10C. The 70:30 sample performed

[a] *Stokes Laboratories, Bernal Institute, University of Limerick, (Ireland)*
[b] *Bernal Institute & Chemical Sciences Department, University of Limerick* † Footnotes relating to the title and/or authors should appear here.
Electronic Supplementary Information (ESI) available: [additional thermogravimetric analysis, structural and electrochemical characterisation].

Table 3. Table comparing the performance of carbon nanofibers in this study to existing literature

Ref	Preparation Method	Potential Window (V)	Number of Cycles (n)	Capacity at nth cycle ($mAhg^{-1}$)
This report	Electrospun from Lignin and PLA or TPU	0.011-3V	500	PLA 50:50- 611 $mAhg^{-1}$ PLA 70:30- 572 $mAhg^{-1}$
[1]	Electrospun PAN/PLLA	0.01–2.80 V	50	435 $mAhg^{-1}$
[9]	electrospun Polypyrrole (PPy) and PAN	0.01 - 2.80 V	50	454 $mAhg^{-1}$
[10]	Electrospun PAN And nitrogen doped PAN	0.01–3.0 V	50	CNFs: ~400 $mAhg^{-1}$ Nitrogen doped- 1150 $mAhg^{-1}$
[21]	PPy precursor, 650 °C activation	0.01 − 3.0 V	600	943 $mAhg^{-1}$
[29]	Electrospun from PAN	0 - 2.8 V	1	450 $mAhg^{-1}$
[32]	multifilament melt-spinning	0- 1.6 V	3	320 $mAhg^{-1}$
[33]	PEO and lignin Electrospinning	0-3 V	50	576 $mAhg^{-1}$
[34]	Pyrolysis and carbonization of Lignin	0.005-1.5 V	65	340 $mAhg^{-1}$
[20]	Electrospun from PAN and N -dimethylformamide (DMF)	0-3V	500	333 $mAhg^{-1}$

slightly better at the highest rates and delivered 245 $mAhg^{-1}$ at a rate of charge/discharge 10C which is more than two and half times what is achievable for graphite, wherein the corresponding capacity is typically well below 100 $mAhg^{-1}$ [40].

Conclusions

Precursor blends of lignin with PLA and TPU were successfully prepared by electrospinning, stabilised and subsequently converted to carbon nanofibers. The addition of MDI promotes crosslinking between the OH group of lignin generating urethane groups, which allow nanofiber shape retention after carbonisation. The compatibility between lignin, PLA and TPU play an important role in the final carbonised CNF morphology. Samples based on TPU produce carbon nanofibres with no porosity while PLA based precursors produce a well-defined porosity. Beyond state of the art capacity values were obtained for nanofibers produced from precursors containing 30% and 50 % PLA and this is attributed to increased porosity levels, leading to additional sites for Li storage. These results provide evidence for the potential of lignin to be valorised in the next generation of LIBs not only in terms of low cost and sustainability point of view but critically in terms of better performance than its petroleum based alternatives.

.

Experimental Section

Materials

Alcell Organosolv hardwood lignin was obtained from Tecnaro GmbH. (Germany). The biobased thermoplastic polyurethane (TPU) was purchased from Veltox (France) (manufactured by Lubriozol). PLA (Ingeo Biopolymer 3001D) injection molding grade was supplied by Natureworks, Minnetonka. Dimethylformamide (DMF), Tetrahydrofuran (THF) and Methylene diphenyl diisocyanate (MDI) were purchased from Sigma Aldrich (Germany).

[a] *Stokes Laboratories, Bernal Institute, University of Limerick, (Ireland)*
[b] *Bernal Institute & Chemical Sciences Department, University of Limerick* † Footnotes relating to the title and/or authors should appear here.
Electronic Supplementary Information (ESI) available: [additional thermogravimetric analysis, structural and electrochemical characterisation].

Table 4. Compositions of the electrospinning solutions

Sample	TcA(g)	PLA (g)	TPU(g)	MDI(g)	DMF (mL)	THF (mL)	Solid content (%)
Lignin/PLA-80:20	2.976	0.8	…	0.224	8.44	8.99	20
Lignin/PLA-70:30	2.604	1.2	…	0.196	8.44	8.99	20
Lignin/PLA-50:50	1.86	2	…	0.14	8.44	8.99	20
Lignin/TPU-80:20	2.976	…	0.8	0.224	18.88	…	20
Lignin/TPU-70:30	2.604	…	1.2	0.196	18.88	…	20
Lignin/TPU-50:50	1.86	…	2	0.14	18.88	…	20

Solution preparation

PLA and TPU based solutions were prepared following the same procedure. PLA was dissolved in a mixture of THF:DMF (1:1 v/v) for 1 hour under magnetic stirring at 50 ºC. TPU was dissolved in the same way only using DMF as solvent. Once PLA or TPU was completely dissolved, lignin was added to the solution. The mixture was homogenised for 30 minutes under magnetic stirring at 50ºC to dissolve lignin completely. Finally, 7 % of MDI with respect to the lignin content was added to the solution and it was kept under stirring for 5 minutes at 50 ºC prior to the electrospinning process. The electrospinning compositions are summarised in Table 4.

Preparation of CNFs

A custom built electrospinner composed of a syringe driver Hardvard PHD 2000 and a power source SIMCO Eurocharger Master were used for producing the nanofibers. The samples were produced at an infusion rate of 30 µl/min. The substrate distance between the needle and the aluminium collector foil was set to 10 cm and the electrospinning was performed at 7.7 Kv. The needle was connected to the power supply and the aluminium foil was ground to the power supply. The Electrospunn Lignin/PLA and Lignin/TPU nanofibers were collected over a copper electrode attached to the aluminium foil. After one hour of electrospinning the copper electrodes were removed from the aluminium foil for the subsequent steps. The CNFs were stabilised in air as follows : temperature was ramped from 25 to 150 °C at 1 °C min^{-1} and kept at 150 °C for 14 h. Then the temperature was raised from 150 °C to 200°C at 1 °C min^{-1} and kept at 200°C for 1 h and then the temperature was ramped again from 200°C to 250°C at 1 °C min^{-1} and kept at 250°C for 1 h. The stabilised Lignin/PLA and Lignin/TPU nanofibres were finally carbonised using a tubular furnace heating from room temperature to 900 °C at 10 °C min^{-1} under nitrogen flow, and kept at 900 ºC for 30 minutes.

Characterization

Scanning Electron Microscopy (SEM) and energy dispersive X-ray spectroscopy (EDS) were performed to determine the nanofiber morphology and the elemental analysis utilizing a Hitachi SU70 microscope coupled to an Oxford Instruments X-Max EDS system at an accelerating voltage of 5 kV and a working distance of 14 mm. The electrodes were placed in a sample holder (ca 2 cm diameter) to study the sample surface. Fourier transform infrared spectroscopy (FTIR) measurements were performed using a Nicolet Nexus FTIR spectrometer over the range 450–4000 cm^{-1}, equipped with an attenuated total reflectance accessory (ATR). A total of 60 scans with a spectral resolution of 2 cm^{-1} were recorded. The Raman spectra of the CNFs were recorded at room temperature in backscattering configuration with a Raman spectrometer (Horiba, LabRAM 1A) equipped with 514 nm laser. The laser was focused to a spot-size of ~10 µm onto the CNF surface using a 50× microscope objective (Olympus). To avoid sample damage, the laser power was limited to a few microwatts. All measurements were calibrated with the spectra of a silicon sample and the spectrometer was kept in the same position to avoid inaccuracy. For the electrochemical characterization, the samples were tested within two electrode Swagelok type cells as the working electrode versus a Li metal counter/reference electrode. All potentials are quoted relative to Li/Li^+. Celgard separators impregnated with a carbonate based electrolyte (1.0 M lithium hexafluorophosphate (LiPF6) solution in ethylene carbonate and diethyl carbonate, battery grade Aldrich) with 3% weight vinylene carbonate (97 % Aldrich) were used. Half-cells were tested galvanostatically between 3-0.011 V (vs Li/Li^+) at C/2 rate (1C= 372 mA/g^{-1}). The potential window was selected to allow comparison with previous carbon nanofiber tests within the literature that use this range [1, 21, 29, 41]. Testing was conducted using a Biologic MPG-2. The cells were assembled and tested within an Ar filled glovebox with O_2 and H_2O levels below 0.1 ppm. The potential carbon yield of the materials was determined using a SETARAM TG-DTA 1600 (Setaram Instrumentation, France), using alumina crucibles. The samples were heated in nitrogen to 900 ºC at a heating rate of 10 ºC/min. Surface area, pores radius and volume values were obtained from nitrogen adsorptiondesorption isotherms by the theory of Brunaeur-Emmett-Teller (BET). The experiments were carried out In an ASAP 2010 (Micromeritics Systems, USA),. The samples were degassed at 200ºC for 12 hours before measurements at 77 K in nitrogen.

Acknowledgements

[a] *Stokes Laboratories, Bernal Institute, University of Limerick, (Ireland)*
[b] *Bernal Institute & Chemical Sciences Department, University of Limerick* † Footnotes relating to the title and/or authors should appear here.
Electronic Supplementary Information (ESI) available: [additional thermogravimetric analysis, structural and electrochemical characterisation].

MC, AB and MNC acknowledge received funding from the BioBased Industries Joint Undertaking under the European Union's Horizon 2020 research and innovation programme under grant agreement No 720707.

Keywords: Lignin • Li-ion batteries • carbon • nanofibers • electrospinning

References

[1] L. Ji, X. Zhang, *Nanotechnology* **2009**, *20*, 155705.
[2] J. Fu, R. Liang, G. Liu, A. Yu, Z. Bai, L. Yang, Z. Chen, *Adv. Mater.* **2018**, 1805230.
[3] C. Wu, X. Tong, Y. Ai, D.-S. Liu, P. Yu, J. Wu, Z. M. Wang, *Nano-micro letters* **2018**, *10*, 40.
[4] B. Dunn, H. Kamath, J.-M. Tarascon, *Science* **2011**, *334*, 928-935.
[5] D. Lin, Y. Liu, Y. Cui, *Nature nanotechnology* **2017**, *12*, 194.
[6] V. Ruiz, A. Pfrang, A. Kriston, N. Omar, P. Van den Bossche, L. Boon-Brett, *Renewable and Sustainable Energy Reviews* **2018**, *81*, 1427-1452.
[7] B. Nykvist, M. Nilsson, *nature climate change* **2015**, *5*, 329.
[8] J. W. Choi, D. Aurbach, *Nature Reviews Materials* **2016**, *1*, 16013.
[9] L. Ji, Y. Yao, O. Toprakci, Z. Lin, Y. Liang, Q. Shi, A. J. Medford, C. R. Millns, X. Zhang, *J. Power Sources* **2010**, *195*, 2050-2056.
[10] D. Nan, Z.-H. Huang, R. Lv, L. Yang, J.-G. Wang, W. Shen, Y. Lin, X. Yu, L. Ye, H. Sun, *J. Mater. Chem. A* **2014**, *2*, 19678-19684.
[11] Y. Lu, L. Yu, X. W. D. Lou, *Chem* **2018**.
[12] G. Huang, F. Zhang, X. Du, Y. Qin, D. Yin, L. Wang, *ACS nano* **2015**, *9*, 1592-1599.
[13] S. Y. Chew, S. H. Ng, J. Wang, P. Novák, F. Krumeich, S. L. Chou, J. Chen, H. K. Liu, *Carbon* **2009**, *47*, 2976-2983.
[14] Z. Xu, Y. Zeng, L. Wang, N. Li, C. Chen, C. Li, J. Li, H. Lv, L. Kuang, X. Tian, *J. Power Sources* **2017**, *356*, 18-26.
[15] Y. Xu, Z. Lin, X. Zhong, B. Papandrea, Y. Huang, X. Duan, *Angew. Chem.* **2015**, *127*, 5435-5440.
[16] J. Sun, H.-W. Lee, M. Pasta, H. Yuan, G. Zheng, Y. Sun, Y. Li, Y. Cui, *Nature nanotechnology* **2015**, *10*, 980.
[17] B. Guo, X. Wang, P. F. Fulvio, M. Chi, S. M. Mahurin, X. G. Sun, S. Dai, *Adv. Mater.* **2011**, *23*, 4661-4666.
[18] C. Xu, D. Niu, N. Zheng, H. Yu, J. He, Y. Li, *ACS Sustainable Chemistry & Engineering* **2018**, *6*, 5999-6007.
[19] R. Thines, N. Mubarak, S. Nizamuddin, J. Sahu, E. Abdullah, P. Ganesan, *Journal of the Taiwan Institute of Chemical Engineers* **2017**, *72*, 116-133.
[20] B. Zhang, Y. Yu, Z. L. Xu, S. Abouali, M. Akbari, Y. B. He, F. Kang, J. K. Kim, *Adv. Energy Mater.* **2014**, *4*, 1301448.
[21] L. Qie, W. M. Chen, Z. H. Wang, Q. G. Shao, X. Li, L. X. Yuan, X. L. Hu, W. X. Zhang, Y. H. Huang, *Adv. Mater.* **2012**, *24*, 2047-2050.
[22] S. Das, *The International Journal of Life Cycle Assessment* **2011**, *16*, 268-282.
[23] M. Culebras, A. Beaucamp, Y. Wang, M. Clauss, E. Frank, M. N. Collins, *ACS Sustainable Chemistry & Engineering* **2018**, *6*, 8816-8825.
[24] N. Dalton, R. P. Lynch, M. N. Collins, M. Culebras, *Int. J. Biol. Macromol.* **2018**.
[25] M. Culebras, M. J. Sanchis, A. Beaucamp, M. Carsí, B. Kandola, A. R. Horrocks, G. Panzetta, C. Birkinshaw, M. Collins, *Green Chemistry* **2018**.
[26] H. Mainka, O. Täger, E. Körner, L. Hilfert, S. Busse, F. T. Edelmann, A. S. Herrmann, *Journal of Materials Research and Technology* **2015**, *4*, 283-296.
[27] E. Frank, L. M. Steudle, D. Ingildeev, J. M. Spörl, M. R. Buchmeiser, *Angew. Chem. Int. Ed.* **2014**, *53*, 5262-5298.
[28] W. Fang, S. Yang, X.-L. Wang, T.-Q. Yuan, R.-C. Sun, *Green Chemistry* **2017**, *19*, 1794-1827.
[29] C. Kim, K. S. Yang, M. Kojima, K. Yoshida, Y. J. Kim, Y. A. Kim, M. Endo, *Adv. Funct. Mater.* **2006**, *16*, 2393-2397.
[30] M. M. Hossain, I. M. Scott, B. D. McGarvey, K. Conn, L. Ferrante, F. Berruti, C. Briens, *J. Anal. Appl. Pyrolysis* **2013**, *99*, 211-216.
[31] S. Gillet, M. Aguedo, L. Petitjean, A. R. C. Morais, A. M. da Costa Lopes, R. M. Łukasik, P. T. Anastas, *Green Chemistry* **2017**, *19*, 4200-4233.
[32] A. P. Nowak, J. Hagberg, S. Leijonmarck, H. Schweinebarth, D. Baker, A. Uhlin, P. Tomani, G. Lindbergh, *Holzforschung* **2018**, *72*, 81-90.
[33] S. X. Wang, L. Yang, L. P. Stubbs, X. Li, C. He, *ACS Appl Mater Interfaces* **2013**, *5*, 12275-12282.
[34] W. E. Tenhaeff, O. Rios, K. More, M. A. McGuire, *Adv. Funct. Mater.* **2014**, *24*, 86-94.
[35] S.-X. Wang, L. Yang, L. P. Stubbs, X. Li, C. He, *ACS applied materials & interfaces* **2013**, *5*, 12275-12282.
[36] J. Jin, B.-j. Yu, Z.-q. Shi, C.-y. Wang, C.-b. Chong, *J. Power Sources* **2014**, *272*, 800-807.
[37] D. S. Knight, W. B. White, *J. Mater. Res.* **1989**, *4*, 385-393.
[38] A. Ferrari, J. Robertson, *Phys. Rev. B* **2001**, *64*, 075414.
[39] C. Kim, S. H. Park, J. I. Cho, D. Y. Lee, T. J. Park, W. J. Lee, K. S. Yang, *Journal of Raman Spectroscopy* **2004**, *35*, 928-933.
[40] S. Sivakkumar, J. Nerkar, A. Pandolfo, *Electrochim. Acta* **2010**, *55*, 3330-3335.
[41] Y. Chen, X. Li, K. Park, J. Song, J. Hong, L. Zhou, Y.-W. Mai, H. Huang, J. B. Goodenough, *Journal of the American Chemical Society* **2013**, *135*, 16280-16283.

[a] *Stokes Laboratories, Bernal Institute, University of Limerick, (Ireland)*
[b] *Bernal Institute & Chemical Sciences Department, University of Limerick* † Footnotes relating to the title and/or authors should appear here.
Electronic Supplementary Information (ESI) available: [additional thermogravimetric analysis, structural and electrochemical characterisation].

Entry for the Table of Contents (Please choose one layout)

Layout 1:

FULL PAPER

The increasing demand for Li ion batteries it makes necessary to develop cost effective and energy efficient materials. The best way to achieve this is utilising sustainable biobased materials. Lignin/PLA nanofibers show enormous potential due their outstanding capacity values and satiability.

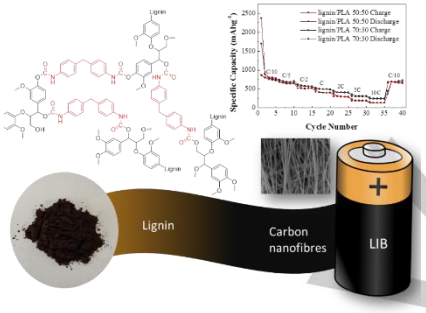

Mario Culebras, Hugh Geaney, Anne Beaucamp, Prathviraj Upadhyaya, Erick Dalton, Kevin M. Ryan and Maurice N. Collins*

Page No. – Page No.

Bio-derived carbon nanofibers from lignin as high performance Li-ion anode materials

[a] *Stokes Laboratories, Bernal Institute, University of Limerick, (Ireland)*
[b] *Bernal Institute & Chemical Sciences Department, University of Limerick* † Footnotes relating to the title and/or authors should appear here.
Electronic Supplementary Information (ESI) available: [additional thermogravimetric analysis, structural and electrochemical characterisation].